

A Data-Driven Model for Aerodynamic Loads on Road Vehicles Exposed to Gusty Bora-Like Winds

Hrvoje Kozmar ^{1,2,*} , Marko Jokić ², Kyle Butler ^{1,3}, Milenko Stegić ² and Ahsan Kareem ¹ 

¹ NatHaz Modeling Laboratory, University of Notre Dame, Notre Dame, IN 46556, USA; kyle.butler@gmail.com (K.B.); ahsan.kareem.1@nd.edu (A.K.)

² Faculty of Mechanical Engineering and Naval Architecture, University of Zagreb, Ivana Lučića 5, 10000 Zagreb, Croatia; marko.jokic@fsb.hr (M.J.); milenko.stegic@fsb.hr (M.S.)

³ The Hartford Steam Boiler Inspection and Insurance Company, Hartford, CT 06102, USA

* Correspondence: hkozmar@fsb.hr

Abstract: Strong cross-wind gusts can cause the vehicle to overturn or slide off the road. This problem is particularly experienced on bridges, as vehicles are extremely sensitive to complex wind-bridge-vehicle interactions. While quasi-steady atmospheric winds create serious difficulties for vehicles, this fact is exacerbated by gusts of wind, as is the case with bora, where gusts of wind can reach velocities five times the average wind velocity. In the present study, experiments concerning aerodynamic loads experienced by vehicles exposed to gusty, bora-like winds are carried out. It is noted that the wind gusting and vortex shedding determine unsteady wind loads on vehicles. The experimental results are used as a basis for developing a simple data-driven modeling approach capable of predicting the time history of aerodynamic loads on vehicles exposed to cross-wind gusts. The modeling results indicate that a model using more than two-state variables is needed to capture the unsteady aerodynamic loads.

Keywords: vehicles; bridges; periodic aerodynamic loads; wind-tunnel experiments; data-driven model



Citation: Kozmar, H.; Jokić, M.; Butler, K.; Stegić, M.; Kareem, A. A Data-Driven Model for Aerodynamic Loads on Road Vehicles Exposed to Gusty Bora-Like Winds. *Appl. Sci.* **2022**, *12*, 7625. <https://doi.org/10.3390/app12157625>

Academic Editor: Wei Huang

Received: 7 July 2022

Accepted: 25 July 2022

Published: 28 July 2022

Publisher's Note: MDPI stays neutral with regard to jurisdictional claims in published maps and institutional affiliations.



Copyright: © 2022 by the authors. Licensee MDPI, Basel, Switzerland. This article is an open access article distributed under the terms and conditions of the Creative Commons Attribution (CC BY) license (<https://creativecommons.org/licenses/by/4.0/>).

1. Introduction

Unsteady aerodynamic loads on vehicles have recently been investigated more closely aiming to improve roadway architecture in order to prevent wind-induced traffic accidents. Along with the development of new experimental and computational techniques, such studies are able to replicate unique flow conditions that were previously beyond the capabilities of traditional wind-tunnel methods. An approach using a conventional wind tunnel capable of generating an impulsive gust from an adjacent shuttered nozzle indicates some practical difficulties (Docton and Dominy, [1]), while a cross-wind track setup in conjunction with a boundary layer wind tunnel shows promising results (Bocciolone et al. [2]). Baker [3] developed a method for the calculation of the time histories of aerodynamic loads experienced by trains for a time domain and artificial gust cases.

The scope of the present study is to investigate gusty bora-like cross-wind loads on vehicles, as observed along the Croatian Coast. Downslope winds with characteristics similar to the Croatian bora are commonly present in many world regions (e.g., Grisogono and Belušić, [4]), so the results of the present study are highly relevant. The experiments concerning aerodynamic loads on vehicles exposed to gusty winds are carried out in a novel wind tunnel and a simple data-driven model capable of predicting the time history of unsteady aerodynamic loads on vehicles is developed. Transient wind effects on engineering structures and vehicles have been widely studied in the past, so the present study is important in supporting further developments on this topic.

3. Experimental Results

Example records of the experimental velocity time series, simulating periodic features of the bora wind, are presented in Figure 2.

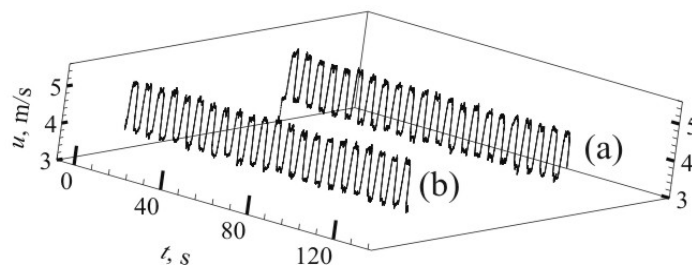


Figure 2. Example velocity time series in accordance with periodic features of the bora wind: (a) model A (without wheels) and (b) model B (with wheels).

Steady aerodynamic loads on the van model increase as the flow velocity increases, Table 1; \bar{u} is average freestream flow velocity. C_{FS} , C_{FL} and C_{MR} coefficients are calculated using the same velocity \bar{u} averaged during low wind periods of the time record ($\bar{u} = 3.8$ m/s).

Table 1. Steady aerodynamic side force, lift force and overturning moment coefficients.

	(a) Low Velocity Period (Weak Winds)					(b) High Velocity Period (Wind Gusts)				
	\bar{u} , m/s	$\sqrt{u'^2}$, m/s	C_{FS}	C_{FL}	C_{MR}	\bar{u} , m/s	$\sqrt{u'^2}$, m/s	C_{FS}	C_{FL}	C_{MR}
Model A	3.8	0.26	0.16	1.21	0.37	5.0	0.38	0.38	2.08	0.68
Model B	3.8	0.26	1.19	0.72	0.46	5.0	0.37	2.14	1.39	0.87

C_{FS} is considerably larger for the B model (with wheels), as the van in that configuration is higher and less protected by the bridge barrier. C_{FL} is larger for the A model (without wheels) due to a stronger flow separation and the respective pressure suction on the roof of the van, when there is no underbody flow. C_{MR} is calculated using the pressure on the sides, and the roof of the van is slightly larger for the B model (with wheels), as in that configuration the contribution to the side force due to higher van model is stronger than the simultaneous reduction in the lift force.

Figure 3a shows the power spectral density of longitudinal velocity fluctuations $f \cdot S_u(f) / \sigma_u^2$ presented against frequency, for the time records presented in Figure 2; f is the frequency, $S_u(f)$ is the power spectral density and σ_u^2 is the variance of the longitudinal velocity.

In Figure 3a, a peak at $f_1 \sim 0.16$ Hz is observed. It is a consequence of intermittent switching between lower and higher flow velocity for 3 s each, which is in accordance with full-scale measurements, a typical feature of bora-like winds. The spectral peak at 0.16 Hz scaled up using the 1:10 time scale would represent wind gusting events lasting 60 s at full-scale. The additional harmonic components are present at $n \cdot f_1$, where $n = 3, 5$, etc., i.e., the first two other harmonics are recorded at 0.48 Hz and 0.8 Hz, a common phenomenon of ideal signals.

The power spectra of longitudinal velocity fluctuations are basically the same in the two studied configurations. In the side force fluctuations, there is a peak at 10 Hz for model A, a trend likely a consequence of vortices shed from the bridge deck, as seen in Figure 3b. For model B, the unsteady aerodynamic side force is predominantly affected by wind gusting because a strong peak at 0.16 Hz, and a less exhibited peak at 10 Hz is observed, as seen in Figure 3b. The flow beneath model B weakens the low-frequency peak in the respective side force spectrum.

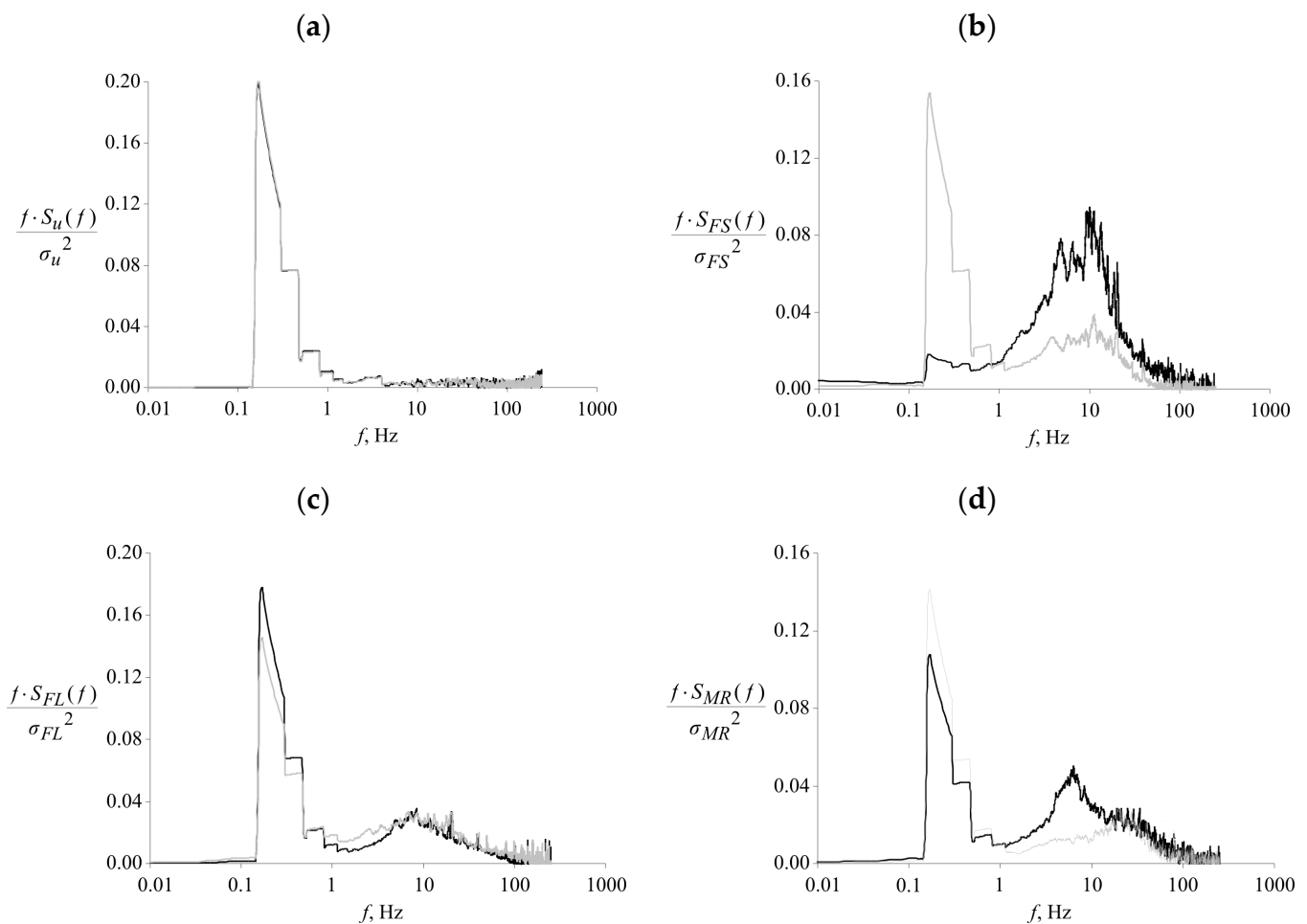


Figure 3. Power spectral density of (a) longitudinal velocity fluctuations, (b) side force fluctuations, (c) lift force fluctuations and (d) overturning moment fluctuations; in all diagrams, the black solid line is for model A and the grey solid line is for model B.

Lift force fluctuations are characterized by a similar trend for both van models, i.e., an exhibited low-frequency peak at 0.16 Hz and a secondary peak at 10 Hz, Figure 3c. The overturning moment for model A is affected by both characteristic flow phenomena, i.e., wind gusting represented by a peak at 0.16 Hz and the vortices shed from the bridge deck, which is observed in the 10 Hz peak. The low-frequency peak at 0.16 Hz is more exhibited for model B, as seen in Figure 3d.

Based on pressure fluctuations observed at the van surface, it is possible to assume that the flow separated from the windward edge of the bridge at frequencies around 10 Hz (1 Hz full-scale) corresponding to the peak in force and moments spectra. The Strouhal number $St = fD/\bar{u}$ is equal to 0.068. It is calculated using the peak frequency $f = 10$ Hz, $D \sim 0.03$ m (bridge-deck model height including the barrier model), and the mean flow velocity $\bar{u} = 4.4$ m/s. $St = 0.068$ is moderately in accordance with full-scale bridge decks because $St \sim 0.1$ is commonly observed regarding flow separation from bridge decks, as shown by Ryall et al. [7].

Previous relevant studies, e.g., Baker [8–10], reported similar results for the overturning moment and the side force, in agreement with the model B (with wheels) reported in the present study. The differences observed for model A are likely a consequence of an overestimation of the lift contribution to the overturning moment because the underbody flow is not present in the model A, in addition to various design features in the leading edge of the bridge model.

4. Modeling Framework

The experimental results are further employed to develop a simple data-driven modeling approach, which is expected to predict the time history of unsteady aerodynamic loads on vehicles in transient winds. To simulate unsteady wind forces on the generic van model, the following linear time invariant (LTI) model (Van Overschee and De Moor [11]) is assumed,

$$\begin{aligned}\dot{\mathbf{x}}(t) &= \mathbf{A}\mathbf{x}(t) + \mathbf{B}\mathbf{u}(t), \\ F(t) &= \mathbf{c}^T\mathbf{x}(t) + \mathbf{d}^T\mathbf{u}(t),\end{aligned}\quad (1)$$

where $\mathbf{A} \in \mathbb{R}^{n \times n}$, $\mathbf{B} \in \mathbb{R}^{n \times 2}$, $\mathbf{c} \in \mathbb{R}^n$ and $\mathbf{d} \in \mathbb{R}^2$ are state matrix, input matrix, output vector and feed-through vector, respectively. Time-dependent vector $\mathbf{x}(t) \in \mathbb{R}^n$ is the state vector, $F(t)$ is the wind-induced force and $\mathbf{u}(t) = (u(t) \ e(t))^T \in \mathbb{R}^2$ is the input vector comprising of wind velocity $u(t)$ and error channel $e(t)$.

The primary motivation for choosing the LTI model for modeling periodic cross-wind loads on a vehicle is its inherent simplicity. Due to the fact that the wind is simulated in laboratory conditions, its spectrum exhibits discrete frequency content. This is unlike bore-like winds in real conditions, where the spectrum is continuous. Indeed, by calculating a discrete Fourier transform of the wind velocity $u(t)$, as seen in Figure 4, dominant harmonic signals are clearly identified at frequencies 0.166 Hz, 0.5 Hz, 0.834 Hz and 1.165 Hz, as that is commonly the case with the ideal signals, where the harmonic components have peaks at 3, 5 and 7 times larger frequencies than the first low-frequency peak.

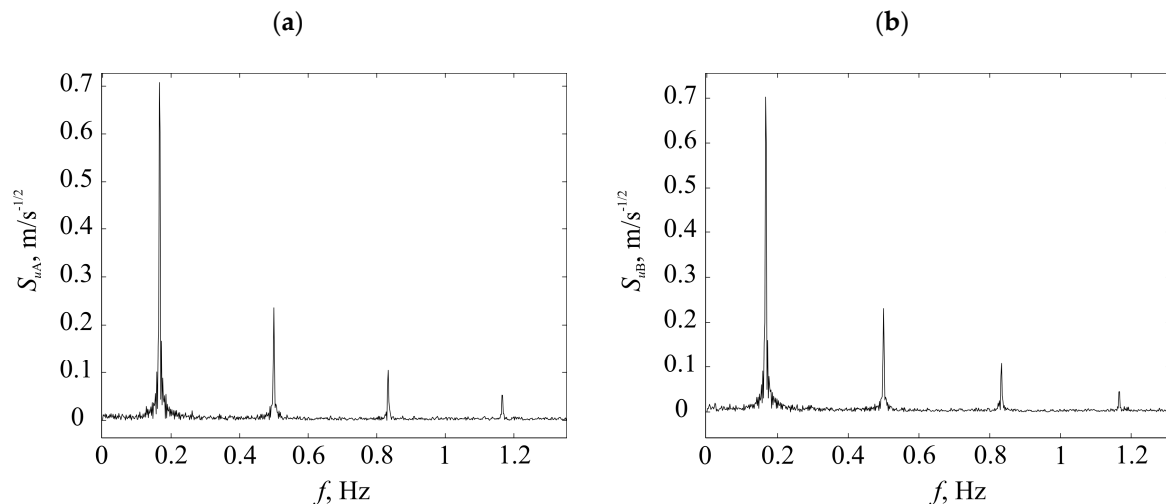


Figure 4. The unfiltered amplitude spectrum of longitudinal velocity fluctuations (discrete Fourier transform of the measured wind velocity): (a) model A and (b) model B.

In Figure 4, the velocity time series is reported in the form of unfiltered amplitude spectrum of longitudinal velocity fluctuations.

Therefore, by calculating discrete Fourier transforms for the unsteady aerodynamic forces experienced by the van model, harmonic signals are observed at the same frequencies, i.e., at frequencies close to 0.166 Hz, 0.5 Hz, 0.834 Hz and 1.165 Hz. As an illustration, the discrete Fourier transform of the unsteady side force is presented in Figure 5.

This provides additional justification for selecting a linear model, i.e., it is well known that the output of a LTI system fed with harmonic signal at a given frequency is also harmonic, with exactly the same frequency content. Thus, this indicates that the measured harmonic signals at the van location, yielding the four discrete frequencies specified above, are due to harmonic wind velocity oscillations only. This serves as a basis for subsequent system identification, i.e., estimation of the unknown model parameters \mathbf{A} , \mathbf{B} , \mathbf{c} and \mathbf{d} .

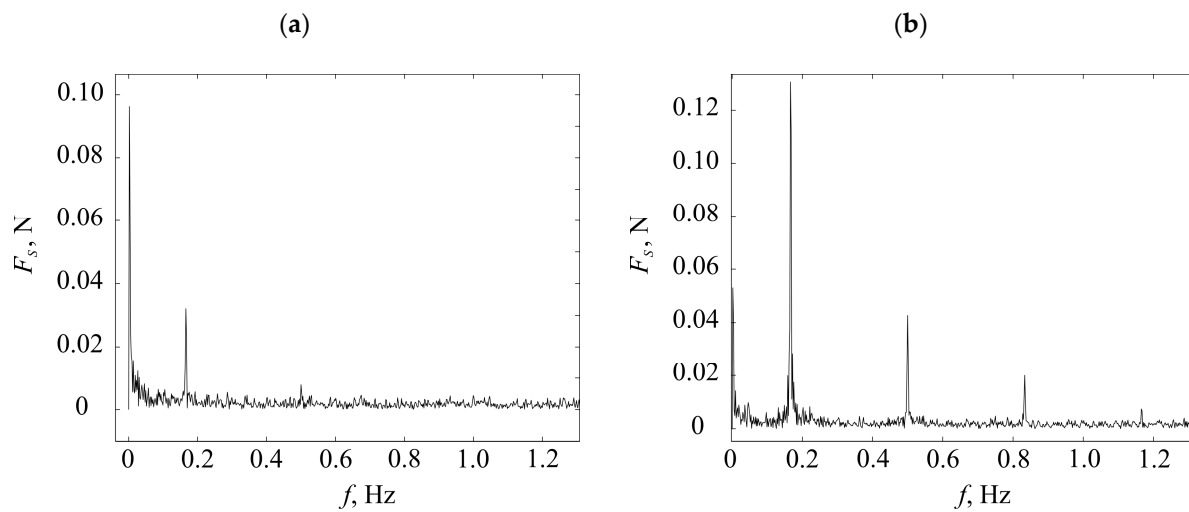


Figure 5. Discrete Fourier transform of the side force determined from the experiment: (a) for model A and (b) for model B.

Prior to this, however, the measured data are pre-processed in the following fashion: Depending upon the transducer position on the vehicle, the measured data also contain signals due to vehicle-induced unsteady flow and vortex shedding, as well as the noise. Such signals are not a direct consequence of wind variations and they present a significant difficulty in system identification. Hence, four band-pass filters centered at the characteristic frequencies are applied to the measured wind force data in order to filter out the spurious signals. For that purpose, second-order digital peaking filters with appropriate bandwidths are used. As a result, wind force data with the desired frequency content are obtained and used in model parameter calculations. This filtering approach generally allows for removing the less relevant content of wind fluctuations.

Finally, the model parameters **A**, **B**, **c** and **d** are estimated using the subspace identification algorithm (Van Overschee and De Moor [11]). For comparison purposes, model parameters were identified for four different model orders $n = 2$, $n = 3$, $n = 4$ and $n = 5$. Due to space constraints, the system matrices are reported for the second-order model only, while the same approach is used to identify the higher order models as well. System matrices for the vehicle models A and B are presented in the Appendix A.

The time-domain response for those models is calculated using the measured wind velocity as the input. In the simulations presented throughout the next section, the error channel is ignored, i.e., $e(t) = 0$ is assumed.

5. Modeling Results

Comparisons of the calculated time-domain model responses and the measured data for the vehicle side force, lift force and overturning moment coefficients are provided in Figures 6–8, respectively.

The modeling results compared against the experimental results indicate that a simple data-driven modeling approach developed in this study is capable of reproducing the time history of periodic aerodynamic loads on vehicles on bridges exposed to cross-wind gusts with satisfactory accuracy. The model with two-state variables is not entirely capable of modeling the van dynamics with sufficient accuracy, i.e., higher-order computational models are required to calculate unsteady aerodynamic loads on vehicles.

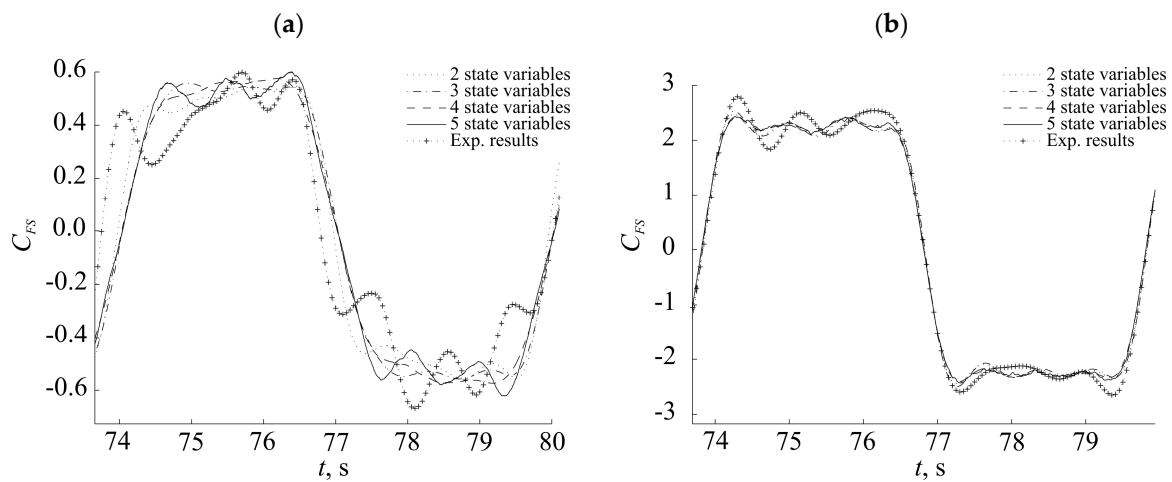


Figure 6. Time history of the side force coefficient; comparison of measured data against calculated time response for two-, three-, four- and five-state variable models for: (a) model A and (b) model B.

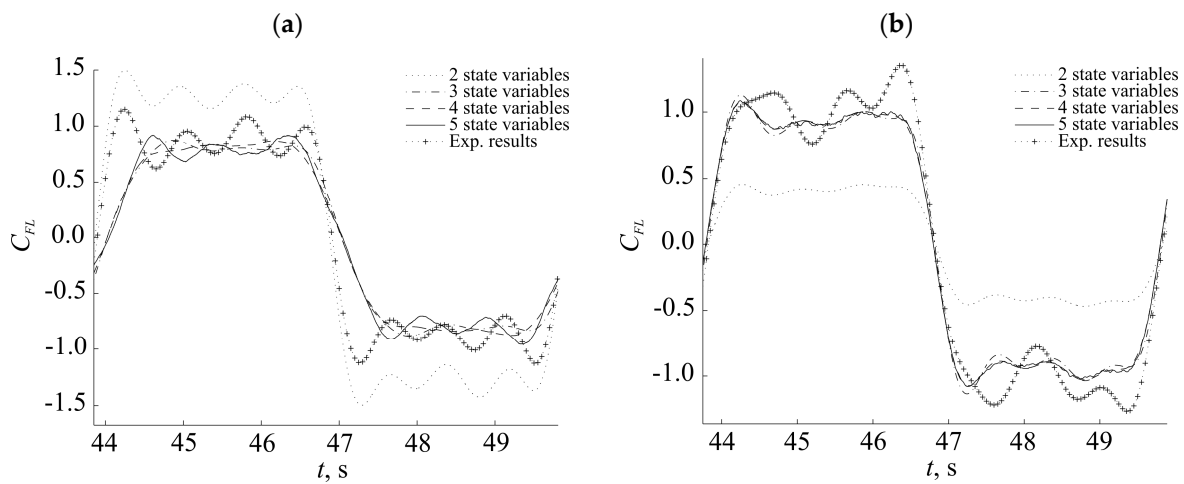


Figure 7. Time history of the lift force coefficient; comparison of measured data against calculated time response for two-, three-, four- and five-state variable models for: (a) model A and (b) model B.

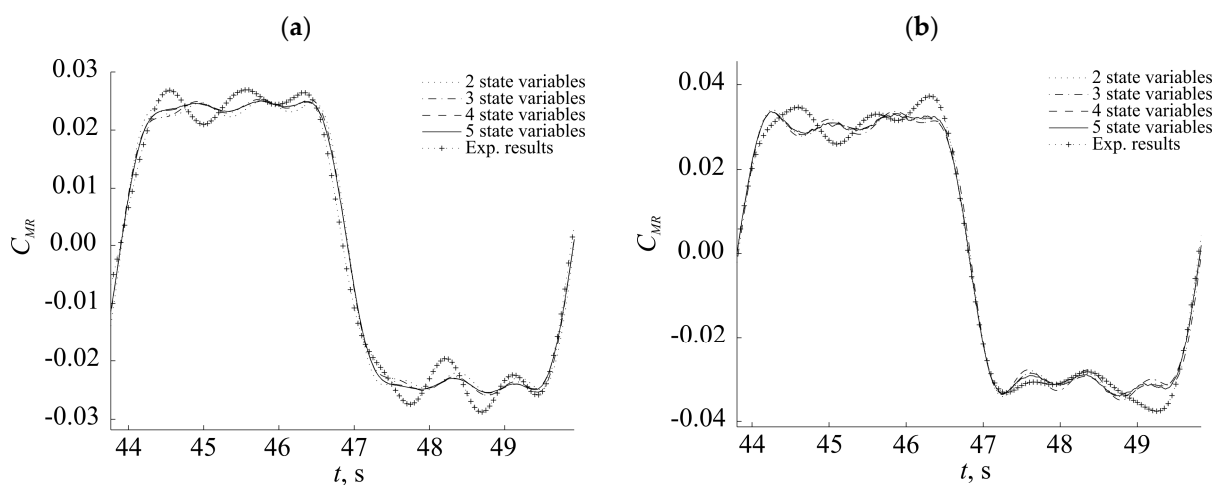


Figure 8. Time history of the overturning moment coefficient; comparison of measured data against calculated time response for two-, three-, four- and five-state variable models for: (a) model A and (b) model B.

6. Concluding Remarks

Wind-tunnel experiments concerning gusty bora-like aerodynamic loads on vehicles are carried out. The focus is on the effects of the vehicle underbody flow on its overall aerodynamics.

Experimental results indicate an increase in steady aerodynamic loads in periods of wind gusts. The steady side force coefficient is larger for the model with wheels, as the vehicle in that configuration is higher and less protected by the bridge barrier. The steady lift force coefficient is larger for the model without wheels due to a stronger flow separation and the corresponding suction pressure on the roof of the vehicle when there is no underbody flow. The steady overturning moment coefficient is slightly larger for the model with wheels.

The experimental results are further used to develop a simple data-driven model capable of predicting unsteady aerodynamic loads on vehicles exposed to cross-wind gusts. The results indicate that a data-driven model using more than two-state variables is needed to fully capture the unsteady aerodynamic loads on vehicles exposed to cross-wind gusts.

The results are constrained by the generic vehicle-bridge system and the studied range of flow velocities, thus outlining the path for future work.

Author Contributions: Conceptualization, H.K., M.J., K.B. and A.K.; methodology, H.K., M.J. and A.K.; software, M.J.; validation, H.K., K.B. and M.J.; formal analysis, H.K., M.J. and M.S.; investigation, H.K., K.B. and M.J.; resources, H.K., M.J. and A.K.; data curation, H.K., M.J. and A.K.; writing—original draft preparation, H.K. and M.J.; writing—review and editing, K.B., M.S. and A.K.; visualization, H.K. and M.J.; supervision, A.K.; project administration, H.K. and A.K.; funding acquisition, H.K. and A.K. All authors have read and agreed to the published version of the manuscript.

Funding: The first author acknowledges the support of the Fulbright Foundation and the NatHaz Modeling Laboratory. Support for Ahsan Kareem and Kyle Butler was provided in part by the Global Center of Excellence, Tokyo Polytechnic University, within the project on load effects in transient flow conditions.

Institutional Review Board Statement: Not applicable.

Informed Consent Statement: Not applicable.

Data Availability Statement: The data presented in this study are available on request from the corresponding author.

Conflicts of Interest: The authors declare no conflict of interest. The funders had no role in the design of the study; in the collection, analyses, or interpretation of data; in the writing of the manuscript, or in the decision to publish the results.

Appendix A

System matrices for the A vehicle model

$$\text{Side force coefficient: } \mathbf{A} = \begin{pmatrix} 0.9989 & -0.01079 \\ 0.0105 & 0.9999 \end{pmatrix}, \mathbf{B} = \begin{pmatrix} -3.521 \cdot 10^{-6} \\ -3.426 \cdot 10^{-5} \end{pmatrix}, \\ \mathbf{c}^T = (4.47 \quad -0.02048), \mathbf{d} = 0$$

$$\text{Lift force coefficient: } \mathbf{A} = \begin{pmatrix} 0.9999 & -0.01039 \\ 0.01077 & 0.9999 \end{pmatrix}, \mathbf{B} = \begin{pmatrix} 6.736 \cdot 10^{-7} \\ -1.385 \cdot 10^{-5} \end{pmatrix}, \\ \mathbf{c}^T = (2.738 \quad -0.01234), \mathbf{d} = 0$$

$$\text{Overturning moment coefficient: } \mathbf{A} = \begin{pmatrix} 0.9985 & -0.01134 \\ 0.009493 & 0.9993 \end{pmatrix}, \mathbf{B} = \begin{pmatrix} 2.375 \cdot 10^{-5} \\ -0.0001701 \end{pmatrix}, \\ \mathbf{c}^T = (0.07229 \quad -0.0003475), \mathbf{d} = 0$$

System matrices for the B vehicle model

$$\text{Side force coefficient: } \mathbf{A} = \begin{pmatrix} 0.9998 & -0.01073 \\ 0.01034 & 0.9997 \end{pmatrix}, \mathbf{B} = \begin{pmatrix} 1.2 \cdot 10^{-5} \\ -2.828 \cdot 10^{-5} \end{pmatrix}, \\ \mathbf{c}^T = (4.843 \quad -0.02205), \mathbf{d} = 0$$

$$\begin{aligned} \text{Lift force coefficient: } \mathbf{A} &= \begin{pmatrix} 0.9998 & -0.01011 \\ 0.009713 & 0.9997 \end{pmatrix}, \mathbf{B} = \begin{pmatrix} 1.32 \cdot 10^{-5} \\ -0.0001077 \end{pmatrix}, \\ \mathbf{c}^T &= (2.32 \quad -0.009992), \mathbf{d} = 0 \\ \text{Overturning moment coefficient: } \mathbf{A} &= \begin{pmatrix} 0.9995 & -0.009959 \\ 0.009483 & 0.9997 \end{pmatrix}, \mathbf{B} = \begin{pmatrix} 2.633 \cdot 10^{-5} \\ -0.0001993 \end{pmatrix}, \\ \mathbf{c}^T &= (0.06171 \quad -0.0002605), \mathbf{d} = 0 \end{aligned}$$

References

1. Docton, M.; Dominy, R. The simulation of transient cross winds on passenger vehicles. In Proceedings of the MIRA International Vehicle Aerodynamics Conference, UK, 1996. Available online: <http://etheses.dur.ac.uk/1580/1/1580.pdf> (accessed on 7 July 2022).
2. Bociolone, M.; Cheli, F.; Corradi, R.; Muggiasca, S.; Tomasini, G. Crosswind action on rail vehicles: Wind tunnel experimental analyses. *J. Wind. Eng. Ind. Aerodyn.* **2008**, *96*, 584–610. [[CrossRef](#)]
3. Baker, C.J. The simulation of unsteady aerodynamic cross wind forces on trains. *J. Wind. Eng. Ind. Aerodyn.* **2010**, *98*, 88–99. [[CrossRef](#)]
4. Grisogono, B.; Belušić, D. A review of recent advances in understanding the meso- and microscale properties of the severe Bora wind. *Tellus* **2009**, *61*, 1–16. [[CrossRef](#)]
5. Kozmar, H.; Butler, K.; Kareem, A. Transient cross-wind aerodynamic loads on a generic vehicle due to bora gusts. *J. Wind. Eng. Ind. Aerodyn.* **2012**, *111*, 73–84. [[CrossRef](#)]
6. Kozmar, H.; Butler, K.; Kareem, A. Downslope gusty wind loading of vehicles on bridges. *J. Bridge Eng.* **2015**, *20*, 04015008. [[CrossRef](#)]
7. Ryall, M.J.; Parke, G.A.R.; Harding, J.E. *The Manual of Bridge Engineering*; Thomas Telford: London, UK, 2000.
8. Baker, C.J. Ground vehicles in high cross winds. 1. Steady aerodynamic forces. *J. Fluids Struct.* **1991**, *5*, 69–90. [[CrossRef](#)]
9. Baker, C.J. Ground vehicles in high cross winds. 2. Unsteady aerodynamic forces. *J. Fluids Struct.* **1992**, *5*, 91–111. [[CrossRef](#)]
10. Baker, C.J. Ground vehicles in high cross winds. 3. The interaction of aerodynamic forces and the vehicle system. *J. Fluids Struct.* **1992**, *5*, 221–241. [[CrossRef](#)]
11. Van Overschee, P.; De Moor, B. *Subspace Identification of Linear Systems: Theory, Implementation, Applications*; Kluwer Academic Publishers: Boston, MA, USA, 1996.